Journal of Drug Delivery Science and Technology 89 (2023) 105070

Contents lists available at ScienceDirect

Journal of Drug Delivery Science and Technology

journal homepage: www.elsevier.com/locate/jddst

Quality by design for the synthesis and optimisation of arginine-poly (ester-amide) nanocapsules as promising carriers for nose-brain delivery of carbamazepine

Noor Mohammed Al-Baldawi [a], Dalia Khalil Ali [b], Qais Jarrar [a], Rasha Abuthawabeh [a], Eman Zmaily Dahmash [c,*]

[a] Department of Applied Pharmaceutical Sciences and Clinical Pharmacy, Faculty of Pharmacy, Isra University, Amman, 11622, Jordan
[b] Department of Physiotherapy Department, Faculty of Allied Medical Sciences, Isra University, Amman, 11622, Jordan
[c] Department of Chemical and Pharmaceutical Sciences, School of Life Sciences, Pharmacy and Chemistry, Kingston University London, UK

ARTICLE INFO

Keywords:
Nanocapsules
Arginine
Interfacial polycondensation
Poly(ester-amide)
Quality by design
Carbamazepine

ABSTRACT

Polymeric nanocapsules for direct brain drug delivery through intranasal is a promising route for drugs that need to reach the brain directly with rapid onset of action and high bioavailability. In this study, arginine-poly(ester-amide) nanocapsules loaded with carbamazepine (CBZ) [(CBZ/Arg-PEA)NCs] were synthesised for direct brain delivery of CBZ via the nose-brain transport pathway using interfacial polycondensation method. Process optimisation was conducted using Quality by Design (QbD) to produce NCs with critical quality attributes (high entrapment and loading efficiencies, low particle size and extended release over 24 h). The design of experiment (DoE) entailed three critical input parameters (CBZ concentration, aqueous, and organic phases volume). The findings of the present study revealed that the optimum formulation would produce high entrapment efficiency (98.6%) and good loading efficiency (20%), targeted release (79% after 24 h) and a small particle size (400 nm). Molecular profiling using FTIR, XRD and DSC showed the formation of the polymer and its semicrystalline nature. TEM images revealed spherical NCs. *In-vivo* study in mice revealed that nose-brain treatment with nanocapsules was capable to deliver CBZ directly to the brain and obtained a sustained increase in brain concentration at 2, 5, and 10 min after the treatment. In conclusion, (CBZ/Arg-PEA) NCs are a promising drug brain delivery system for treating epilepsy via the nose-brain transport pathway.

1. Introduction

Polymeric nanoparticles are promising drug delivery systems with several biological advantages due to their smaller size. They can rapidly cross the physiological barriers and reach the target sites at sufficient drug concentrations. In addition, their use is generally associated with fewer adverse effects when compared to many other drug delivery systems [1–4]. The use of a polymeric nanocapsules delivery system, nevertheless, requires the control of several features of the polymeric nanocapsules such as their composition, entrapment efficiency, loading efficiency, size distribution, drug release profile and stability [2–8]. Several factors, especially parameters used in the synthesis procedures, have dramatic effects on the quality and effectiveness of particular nanocapsules samples. For pharmaceutical applications, polymeric nanocapsules should have high entrapment efficiency or loading capacity, narrow size distribution, and long-term stability. However, for medical and therapeutic use, these nanocarriers should exhibit some advantages in term of biosafety and their capability to provide targeting delivery with sustained release of entrapped drugs [1,6,9–14].

The use of Arginine-based poly(ester-amide)s (Arg-PEA)s in nanocapsules synthesis may provide a preferable feature in term of biocompatibility, biodegradability and their capability to penetrate cell membrane with low cytotoxicity. It has various applications, for example, non-viral gene carriers, bone tissue engineering, carriers for nucleic acid drugs, and (Arg-PEA)s also can promote transdermal delivery of insulin [15–25]. Interfacial polycondensation was considered the main method for forming nanoencapsulation products. Therefore, many parameters were investigated to see how they affected particle

* Corresponding author. Department of Chemical and Pharmaceutical Sciences, School of Life Sciences, Pharmacy and Chemistry, Kingston University London, Kingston upon Thames, KT1 2EE, UK.
E-mail address: e.dahmash@kingston.ac.uk (E.Z. Dahmash).

https://doi.org/10.1016/j.jddst.2023.105070
Received 8 June 2023; Received in revised form 30 September 2023; Accepted 14 October 2023
Available online 15 October 2023

size and particle size distribution. These parameters are organic/aqueous phase ratio, the concentration of emulsifier, the concentration of the drug, and core/wall ratio [14,26–30].

Quality by Design (QbD) is a strategic development and optimisation method in several industries including the pharmaceutical [31]. It aimed to ensure that a final drug product's intended performance in both terms of safety and effectiveness is as predicted. The QbD concept is based on key elements and stages. The first stage is defining the quality target product profile (QTPP), identifying important properties that need to be within the final product. The second stage involves determining the critical quality attributes (CQAs), which refer to the set of the QTPP that are critical and requires to be controlled to ensure product safety and effectiveness. The third one is setting the critical input/process parameters (CPP) that define the factors that might affect the product CQAs. The final stage is choosing a mathematical model using design of experiment (DoE) tool, identifying relevant design and control spaces for picking the optimum formulation, and proposing a control approach for ongoing improvement [31–37].

Carbamazepine, a common active pharmaceutical ingredient (API), is a frequently used drug as a first-line treatment for epilepsy and generalized tonic-clonic or partial seizures. However, treatment with oral CBZ is associated with several drawbacks that dramatically limit its clinical uses. Treatment with oral CBZ has been associated with delayed onset of therapeutic action and extensive first pass metabolism. A couple of evidence also demonstrated that oral CBZ is a potent inducer of drug-metabolizing enzymes and therefore, increases the potential risk of drug-drug interaction [38–41]. Therefore, an alternative intranasal route has been investigated to improve the efficacy and minimize the toxicity of antiepileptic drugs by delivering the drug directly to the brain via the olfactory route and hence requiring a much lower dose, which may result in reduced toxicity and side effects. As a result, CBZ could be administered nasally to take advantage of the nose-brain route [40,42,43].

A handful of separate studies have suggested a significant impact of polymeric nanocapsules in improving the therapeutic activity of candidate and existing drugs as well as reducing their gastric and systemic toxicities. However, no study has yet investigated the potential of polymeric nanocapsules in enhancing CBZ delivery to the brain for rapid management of seizure attacks. Accordingly, the present study was conducted with an attempt to employ QbD to synthesise and optimise the formulation of (CBZ/Arg-PEA) nanocapsules (NCs) as a promising drug brain delivery system via the nose-brain route of administration. With this regard, we hypothesized that intranasal administration of polymeric nanocapsules of CBZ is capable to take the CBZ directly to the brain and avoid the delayed effect.

2. Materials and methods

2.1. Materials

Carbamazepine (CBZ) powder, Pentylenetetrazol (PTZ) and Diazepam (DZP) were obtained from Sigma Aldrich (Pool, UK), L-arginine amino acid and glycerine were purchased from Labchem (Schaumburg, IL, USA). Cis/*trans*-1,4-cyclohexanediol was purchased from Thermo Fisher Scientific (Dratford, United Kingdom). Potassium hydroxide pellets (KOH) were obtained from Riedel-de Haën (Seezle, Germany). Terephthaloylchloride, dimethylsulfoxide (DMSO), dimethylformamide (DMF), dimethylacetamide (DMA), sodium carbonate (Na_2CO_3) and p-toluene sulfonic acid monohydrate were obtained from Acros Organics (Geel, Belgium). Chloroform ($CHCl_3$), trifluoroacetic acid (TFA), toluene (C_7H_8), acetone (C_3H_6O) and HPLC grade acetonitrile (CH_3CN) were obtained from Alpha Chemika (Maharashtra, India). HPLC grade methanol (CH_3OH), diethyl ether $(C_2H_5)_2O$, perchloric acid ($HClO_4$) and HPLC grade water (H_2O) were obtained from Tedia high purity solvents (Fairfield, CT, USA).

2.2. Di-p-toluene sulfonic acid salt of O, O′-bis-(L-arginine ester)-cis/trans-1,4-cyclohexanemonomer

L-arginine (40 mmol, 6.96 g), Cis/*trans*-1,4-cyclohexanediol (20 mmol, 2.32 g), and *p*-toluene sulfonic acid monohydrate (40 mmol, 7.6 g) in 150 mL of toluene were placed in a 250 mL round-bottomed flask processed with a Dean-Stark trap and a condenser. The reaction mixture was heated to reflux for 10 h. The reaction mixture was then cooled to room temperature; toluene was removed by suction filtration and washed with acetone. The product was dried at 60 °C under vacuum for 10 h. The final product was obtained as a white solid (92% yield).

2.3. Synthesis of poly(ester-amide) based on L-arginine (Arg-PEA)

Di-p-toluene sulfonic acid salts of O, O′-bis-(L-arginine ester)-cis/*trans*-1,4-cyclohexane monomer (5 mmol, 4.23 g) and KOH (10 mmol, 0.56 g) were dissolved in (20 mL) of distilled water and placed in a 100 mL round-bottomed flask. Terephthaloylchloride (5 mmol, 1.00 g) was dissolved in (10 mL) chloroform and added to the prepared aqueous solution dropwise over 4 min at room temperature with vigorous stirring for 30 min. The formed polymer was filtered and washed with distilled water. Polymer drying was accomplished using freeze drying for 10 h to remove solvent residue.

2.4. Synthesis of poly(ester-amide) based on L-arginine loaded with CBZ nanocapsules [(CBZ/Arg-PEA) NCs]

The preparation of (CBZ/Arg-PEA) NCs was based on the method employed for the synthesis of the poly(ester-amide) [sections 2.2 and 2.3]. The only difference is that the designated amount of **c**arbamazepine was added to the chloroform **(**$CHCl_3$**)**.

2.5. Characterisation

2.5.1. Solution viscosity

The dilute solution viscosity of the (Arg-PEA) NCs was measured using an automated microviscometer (Anton Paar Ltd., St Albans, UK). A 1.8 mm capillary tube was employed in the measurement with a 1.5 mm steel ball (density 7.7 g/cm^3) and an inclination angle of 80°. The viscometer was calibrated with the viscosity standard N26 from Paragon Scientific Ltd. (Birkenhead, UK). The experiment was run at 25 ± 0.1 °C. Measures were repeated five times and reported as mean ± standard deviation (SD) [44].

2.5.2. Molecular weight measurement

The molecular weight of the produced polymer (Arg-PEA) was measured in aqueous suspension by dynamic light scattering using a Nicomp N3000 (Billerica, USA).

2.5.3. Fourier transform infrared (FTIR) spectroscopy analysis

FTIR spectra of the monomer (Arg-PEA) and (CBZ/Arg-PEA) NCs samples were recorded using Perkin Elmer FTIR spectrometer (OH, USA), coupled with Spectrum 10 software that was used to operate and treat FTIR spectra. A sample of few milligrams was loaded on the sample holder above a laser lens and held in place by screwing down the relevant adaptor. Each sample's FTIR spectrum scans were obtained over the range of 450–4000 cm^{-1} with a resolution of 2 cm^{-1}.

2.5.4. Nuclear magnetic resonance (NMR) spectroscopy

The ^{1}H NMR and ^{13}C NMR of the prepared monomer and (Arg-PEA) were recorded on a Bruker 500 MHz spectrometer (Bruker DPX-500) using tetramethylsilane (TMS) as the internal standard.

2.5.5. Differential scanning calorimetry (DSC) analysis

DSC analysis of CBZ, (Arg-PEA) and optimal (CBZ/Arg-PEA) NCs formulation was carried out using DSC Q200- TA instrument (USA).

Table 1
List of factors (CPP) and responses (CQA) with their details that were used in the DoE study.

Name	Abbr.	Units	Type	Settings
Factors (CPP)				
API-Conc.	API	%	Quantitative	−1, 0, 1
Aqueous Volume	AQU	mL	Quantitative	−1, 0, 1
Organic Volume	ORG	mL	Quantitative	−1, 0, 1

Name	Abbr.	Units	Type	Min	Target	Max
Responses (CQA)						
Entrapment Efficiency	EE	%	Regular	50	70	90
Loading Efficiency	ENC	%	Regular	20	30	40
Particle Size	PSA	nm	Regular	100	300	500
Percentage released	REL	%	Regular	40	60	80

Table 2
Summary of the concentrations of CBZ, aqueous and organic media volumes that were employed in the DoE study highlighting the lower (−1), medium (0) and the higher (1) concentrations.

Factor	−1	0	1
API concentration	100 mg	300 mg	500 mg
Aqueous Volume	10 mL	20 mL	30 mL
Organic Volume	10 mL	20 mL	30 mL

Table 3
Animal grouping description for the nose-brain *in vivo* study.

Group	Treatment	Exposure time
Control Group I (6 mice)	Drug-Free nanoparticles (Arg-PEA)	30 s (30 s before sacrificing)
Control Group II (6 mice)	Drug-Free nanoparticles (Arg-PEA)	Two minutes before sacrificing
Control Group III (6 mice)	Drug-Free nanoparticles (Arg-PEA)	Five minutes before sacrificing
Control Group IV (6 mice)	Drug-Free nanoparticles (Arg-PEA)	Ten minutes before sacrificing
Test Group I (6 mice)	(CBZ/Arg-PEA) NCs	30 s (30 s before sacrificing)
Test Group II (6 mice)	(CBZ/Arg-PEA) NCs	Two minutes before sacrificing
Test Group III (6 mice)	(CBZ/Arg-PEA) NCs	Five minutes before sacrificing
Test Group IV (6 mice)	(CBZ/Arg-PEA) NCs	Ten minutes before sacrificing

Around 2.5 mg sample was placed onto an aluminium pan and heated at a heating rate of 10 °C/min under continuous nitrogen purging (50 mL/min).

2.5.6. Particle size determination

The average diameter of (Arg-PEA) and (CBZ/Arg-PEA) NCs was analysed at 25 °C by Photon correlation spectroscopy using a Zeta sizer Nano ZS90 (Malvern Instrument, UK). Before analysis, samples were diluted with HPLC grade distilled water, sonicated at medium amplitude (~50 Hz) for 40 s. The analysis was performed in triplicate and results for the QbD study were recorded as mean.

2.5.7. Scanning electron micrographs (SEM)

Surface topography was examined for (Arg-PEA) and (CBZ/Arg-PEA) NCs using JSM-IT300 (JEOL, Japan). Around 3 mg of each sample were sprinkled on a double-adhesive carbon tape affixed to an aluminium tub. Samples were analysed without any further coating.

2.5.8. Transmission electron microscopy (TEM)

One drop of fresh ((CBZ/Arg-PEA) NCs dispersion was put on Formvar-coated copper grids (300 mesh, Electron Microscopy Sciences, Hatfield, PA, USA). Imaging was accomplished on an FEI Morgagni 268 TEM (Eindhoven, Netherlands).

2.5.9. X-ray diffraction (XRD) analysis

X-ray diffractometry (MiniFlex 600 benchtop diffractometer (RigaKu, Tokyo, Japan)) was used to investigate the physical form of CBZ, (Arg-PEA) and (CBZ/Arg-PEA) NCs. The XRD experiments were performed over the range 2θ from 5 to 99°, with Cu Kα radiation (1.5148227 Å) at the voltage of 40 kV and a current of 15 mA. All samples were fixed on a glass holder and scanned in triplicate. Data were recorded at a scanning speed of 5°/minute. OriginPro® software was employed to analyse the scans (OriginLab Corporation, USA).

2.5.10. High-performance liquid chromatography (HPLC)

HPLC method was employed for the quantitative analysis of CBZ. A Dionex Softron HPLC System from Thermo Fisher Scientific Inc., with gradient pump, UV detector set at 285 nm coupled with Fortis-C18 analytical column (Fortis technologies Ltd C 18. 250 × 4.6 mm) were used. The mobile phase was composed of acetonitrile: 0.125% TFA in water with a ratio of (80: 20 v/v). The run time was 10 min, and the sample temperature was off while the column temperature was set at 20 °C. The flow rate was set at 0.5 mL/min, with a sample injection volume of 20 μL. The HPLC method was validated according to ICH guidelines in terms of specificity, accuracy, precision, linearity, detection limits, and quantification [45].

2.5.11. Content uniformity

About 100 mg from each produced formula was weighted using Bel Engineering balance (Italy), dissolved in 50 mL DMSO with vigorous stirring for 15 min, sonicated for 20 min, then filtered using a syringe membrane filter (0.22 μm) and injected in the HPLC to quantify CBZ content.

2.6. Quality by design (QbD) analysis

2.6.1. Elements of QbD

Based on initial screening studies and literature review of the interfacial polymerization process, the critical quality attributes (CQA/response) were selected for optimisation using the critical input parameters (CPP/factor). The CPPs were set as key factors to include in the DoE investigation. The factors were the CBZ quantity, aqueous medium volume, and organic medium volume. Furthermore, CQAs or responses were entrapment efficiency, loading efficiency, the nanoparticles particle size, and percentage release of CBZ after 24 h.

2.6.2. Design of experiment (DoE)

MODDE software version 12.1 (Umetrics Inc., Sweden) was employed to design the DoE study. A Central Composite Design (CCF) of the DoE with a quadratic model was selected, which was further fitted using the partial least squares (PLS) method. Whereas response surface modelling (RSM) was employed to investigate and optimise the non-linear multidimensional relationship between factors and responses. A total of 17 CBZ containing formulations were proposed by the software, that include triplicate runs, to evaluate the reproducibility of the model. The experiments were prepared and tested according to the suggested run order given by the software to ensure the randomness of the process. Table 1 presents the factors/CPP and the responses/CQA which were used in the DoE study.

In this project, none of the factors or responses' values were transformed, and thus the type is considered regular. However, for factors, the settings for the upper and lower limits of used quantities were encoded as −1, 0, or 1 that stands for the lowest value, intermediate value, and highest value, respectively. Values of input parameters are summarized in Table 2. The software generated the experiments' list, run order, and composition.

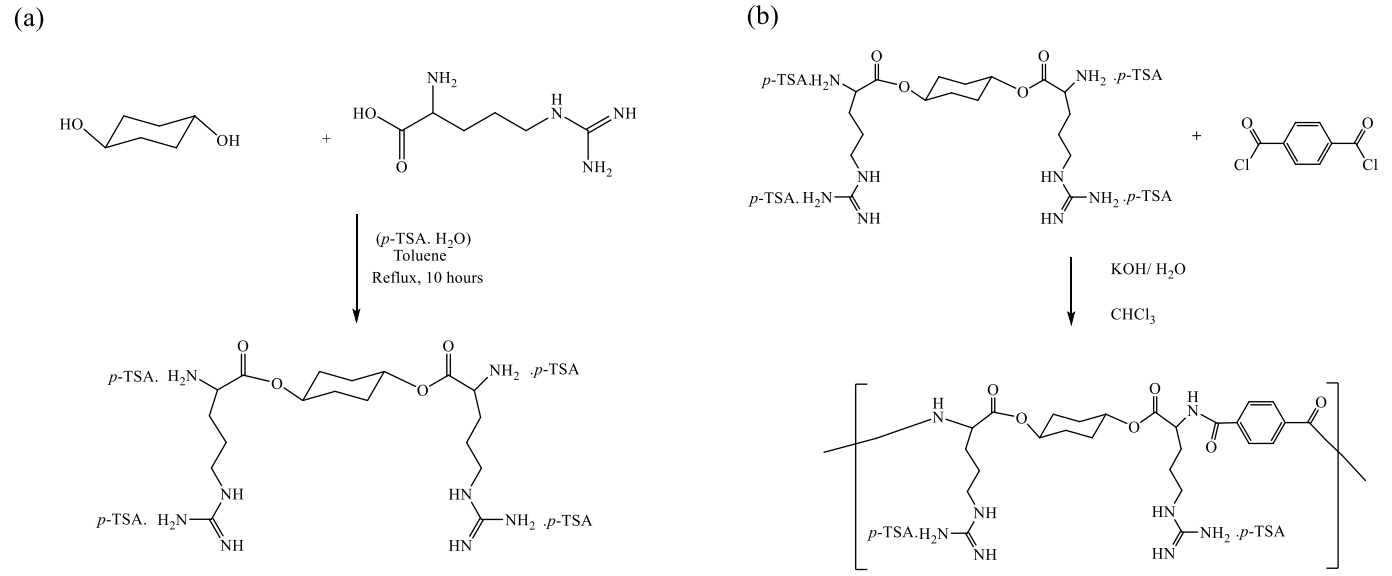

Fig. 1. (a) Di-p-toluene sulfonic acid salts of O, O′-bis-(L-arginine ester)-cis/*trans*-1,4- cyclohexane monomer (b) Synthesis of poly(ester amide)s by interfacial polycondensation of di-p-toluene sulfonic acid salts of O, O′-bis-(L-arginine ester)-cis/*trans*-1,4- cyclohexane monomer.

2.6.3. Model verification

Model verification was accomplished in a stepwise pattern. Several plots were employed for that, such as, Distance to Model Plot in which exclusion of the most relevant outlier experiments from the model took place, and model fitting plot. After that, insignificance model terms that negatively affect the model prediction power were excluded.

2.6.4. Analysis of variance (ANOVA)

ANOVA was employed to assess the significance and validity of the model. Two main components were evaluated for that. The first is the model regression variations with significance means a p-value of less than 0.05. The second one is the variance that is attributed to residuals and replicate errors denoted by the p-value of the model error (lack to fit). Significant model is the one with lack of fit value is higher than 0.05. Then, according to regression coefficient values, all insignificant terms were determined and eliminated to reveal the regression equations for all CQA.

2.6.5. Entrapment efficiency and loading efficiency

Different formulas of (CBZ/Arg-PEA) NCs were formulated. Each one was prepared by varying the amount of the aqueous media (distilled water), the organic media (chloroform), and CBZ. The experiments used lower, medium, and higher amounts of each factor (aqueous, organic, and CBZ) which will enable the selection of the most optimal procedure that delivers targeted CQA. Each formula was prepared using the same procedure of preparing the (CBZ/Arg-PEA) NCs as discussed earlier. Each powder yield was dried using a freeze dryer for at least 15 h and then sieved through sieve with aperture of 32 μm to break agglomerates. For each of the experiments the entrapment efficiency (EE%), loading efficiency (LE%) were calculated according to equations (1) and (2) respectively:

$$\mathrm{EE}\ (\%) = \frac{\mathrm{CBZ_t} - \mathrm{CBZ_f}}{\mathrm{CBZ_t}} \times 100 \qquad \text{Eq (1)}$$

$$\mathrm{LE}\ (\%) = \frac{\mathrm{CBZ_t} - \mathrm{CBZ_f}}{\mathrm{Formula}} \times 100 \qquad \text{Eq(2)}$$

Where CBZ_t is the total amount of CBZ added to the formula, CBZ_f is the total amount of CBZ collected from the filtrates, and "Formula" is the total amount of the produced (CBZ/Arg-PEA) NCs.

2.6.6. Release study

A total of 5 mg from each (CBZ/Arg-PEA) NCs formula was weighed and used with UV-VIS spectrophotometer (Microplate spectrophotometer Thermo Fisher, Finland) for in vitro release study. The amount of formula was placed in a UV cuvette with 3 mL of phosphate buffer saline pH 6.8. The UV spectrometer was set at a wavelength of 285 for 24 h with readings taken every 10 min. The amount of the formula was selected to ensure the saturation solubility of CBZ was not reached (solubility is 503.9 μg/mL in phosphate buffer pH 6.8 [46]). The cumulative amount of the released CBZ was measured at pre-set time intervals at the corresponding λ-max. The method was calibrated using PBS and a calibration curve was constructed over a range of 3.125–62 μg/mL. To ensure sink conditions were maintained, the release of carbamazepine alone (1.5 mg) was evaluated using the same method. Fig. S1. showed a complete dissolution of CBZ within 5 h (>90% in 4 h).

2.7. In-vivo evaluation

2.7.1. Animal care and husbandry

A total of 88 Swiss albino male mice, weighing between 25 and 30 g were used in this study. The mice were bred and raised in the animal facility at Isra University in Jordan. They were housed under controlled environmental conditions, maintaining a temperature of 22–25 °C, relative humidity between 67 and 77%, and a 12/12-h light/dark cycle. The mice were provided with polypropylene cages (30 × 22 × 16 cm^3) and had free access to food and water. All animal handling and experimental procedures were performed in accordance with the guidelines of the Institutional Animal Care and Use Committee (IACUC), and the study received approval from the Scientific Research Ethics Committee at Isra University (SREC/23-19/2020/2021).

2.7.2. HPLC brain analysis

The primary objective of this brain targeting study is to investigate the presence and concentration of CBZ in the brain tissue following the administration of (CBZ/Arg-PEA) NCs to mice via a nose-only inhalation apparatus. To achieve this, the mice were divided into eight groups, each comprising 6 mice. Among these groups, four control groups (Control Group I to IV) were designated to receive drug-free nanoparticles (Arg-PEA), while the other four test groups (Test Group I to IV) received (CBZ/Arg-PEA) NCs. Each group was exposed to the respective NCs at different time intervals before the mice were sacrificed for brain tissue

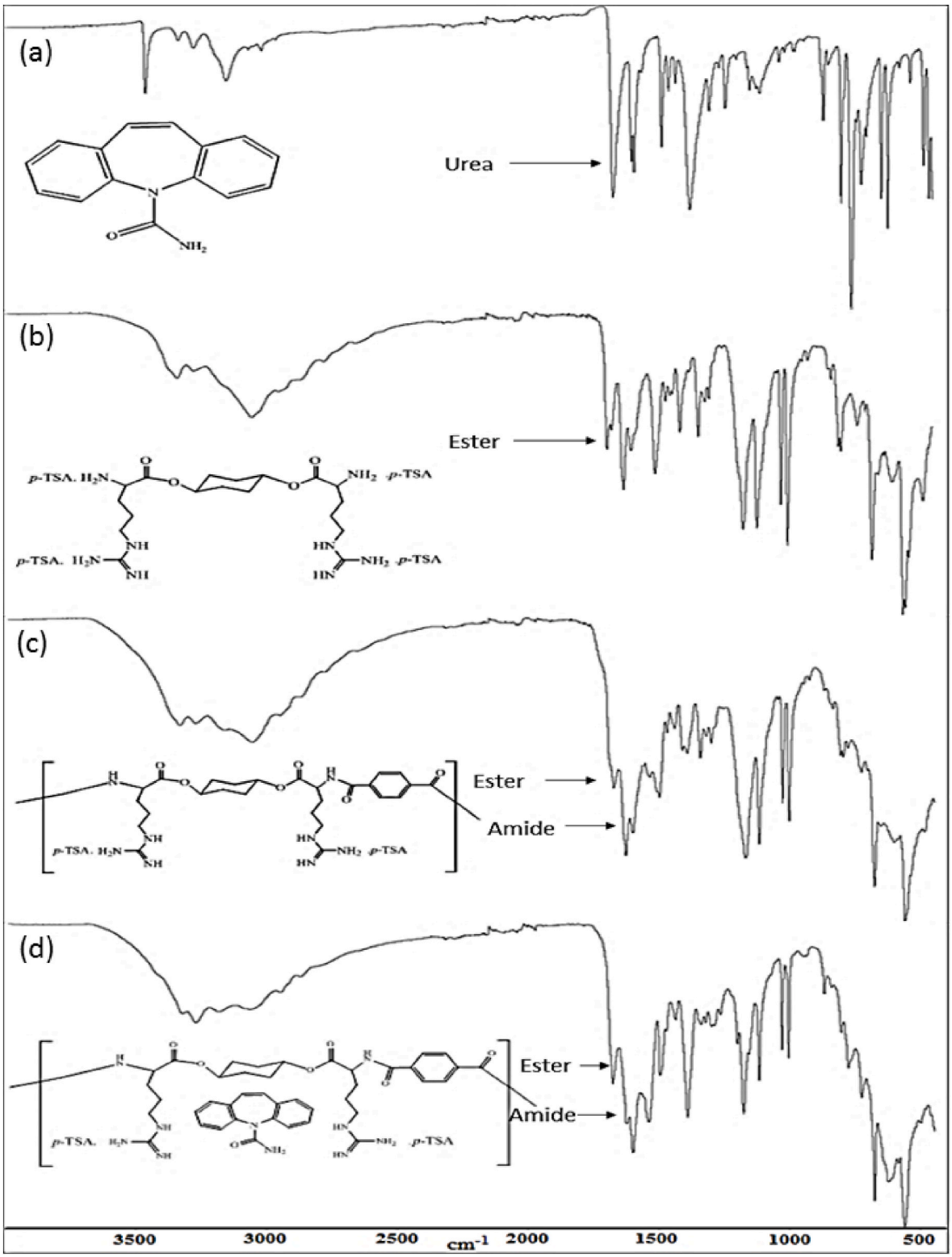

Fig. 2. FTIR spectra of (a) CBZ (b) di-p-toluene sulfonic acid salt of O,O′-bis-(L-arginine ester)- cis/trans monomer, (c) (Arg-PEA), (d) (CBZ/Arg-PEA) NCs.

analysis as described in Table 3. To conduct the experiments, a nose-only inhalation apparatus was used. This specialized apparatus consists of a 15-mL centrifuge (Falcon) tube with a hole for a delivery port on the wall, a hole for air inlet tube on the tapering portion, air inlet tube, pipette bulb and receptacle (tube cap) for drug powder [47]. The receptacle was filled with 1.00 g of sample powder before dosing of each animal. During the dosage, the mouse nose was inserted shortly in the delivery port. The pipette bulb was squeezed and released once every 10 s for three times to aerosolize NCs powder and create a 'dusty' atmosphere for the animal to breathe.

The animal was sacrificed by cervical dislocation, and the brain was collected, weighted, and kept in the refrigerator at – 80 °C for subsequent investigations. Each brain was homogenized in HPLC water using a homogenizer at a ratio of 1:2 (w/v) and then centrifuged at 20 °C with

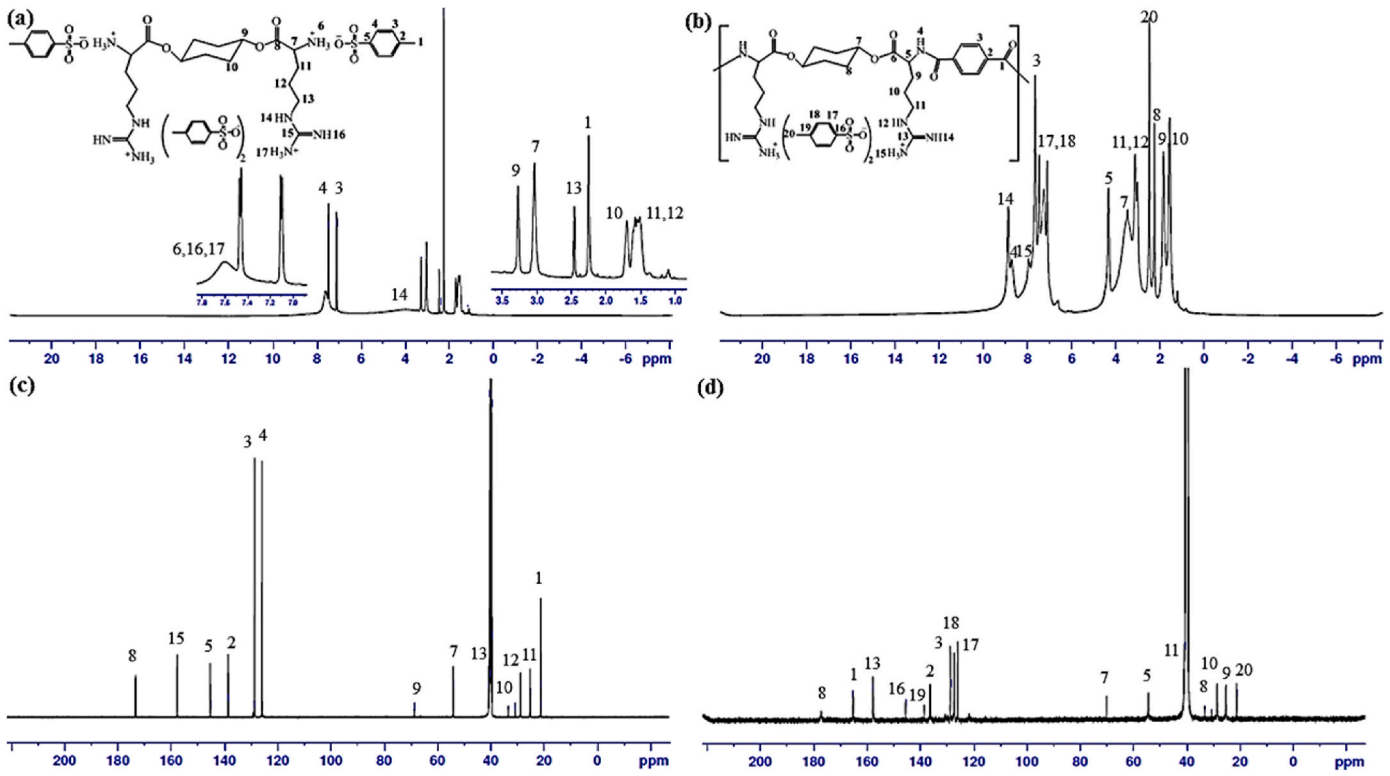

Fig. 3. (a)^{1}H NMR of di-p-toluene sulfonic acid salt of O,O′-bis-(L-arginine ester)- cis/trans 1,4-cyclohexane monomer, (b) ^{1}H NMR of poly-(ester amide) based on L-arginine, (c) ^{13}C NMR of di-p-toluene sulfonic acid salt of O,O′-bis-(L-arginine ester)- 1,4-cyclohexane monomer (d) ^{13}C NMR poly (ester amide) based on L-arginine.

10,000 rpm for 10 min. The supernatant was then refrigerated at −70 °C until HPLC analysis was performed. For HPLC analysis, a predetermined amount of each sample (200 μL) was treated with 50 μL diluted perchloric acid (1.195 in 100 mL distilled water), mixed thoroughly, and centrifuged at 10,000 rpm for 10 min at 20 °C to remove all brain tissue residuals. The supernatant was then diluted with 0.5 mL acetonitrile and filtered before injected in HPLC [42].

2.7.3. Anticonvulsant evaluation

For the anticonvulsant test, a randomized allocation of mice into five groups (n = 8) was performed using a previously described procedure [48–50]. The experimental protocol involved the following treatments: Group I served as the Vehicle Control group, receiving a solution containing 2% dimethyl sulfoxide (DMSO) in saline. Group II received treatment with a drug free polymer, exposed to three puffs of (Arg-PEA) NCs. Groups III and IV were designated as Standard groups and received reference drugs, namely DZP (1 mg/kg orally) and CBZ (25 mg/kg orally) respectively. Group V, referred to as the Test group, was exposed to three puffs of (CBZ/Arg-PEA) NCs.

All drug administration took place 15 min prior to the administration of PTZ (80 mg/kg, intraperitoneally), which was used to induce seizures in the mice. Subsequently, the mice were placed in Plexiglas cages (each measures 30 × 22 × 16 cm) and subjected to a 30-min observation period, during which the latency of seizure onset and the duration of seizures were recorded. Additionally, the intensity of seizures was assessed using a modified Racine scale, involving the following scoring criteria: 1 - Mouth and facial movements; 2 - Head nodding; 3 - Forelimb clonus; 4 - Rearing; 5 - Rearing and falling. The inclusion of PTZ allowed for the evaluation of the anticonvulsant effects of the various treatments and the measurement of seizure parameters. Statistical significance was detected using Tukey's test, with p-value less than 0.05, as analysed with GraphPad Prism. Results were reported as mean ± standard error of mean (SEM).

3. Results and discussion

3.1. Synthesis of di-p-toluene sulfonic acid salts of O, O′-bis-(L-arginine ester)-cis/trans-1,4- cyclohexane monomer

Di-p-toluene sulfonic acid salts of O, O′-bis-(L-arginine ester)-cis/*trans*-1,4- cyclohexane monomer was successfully synthesised. In addition, 1,4-cyclohexanediol was condensed with L-arginine amino acid in a nonpolar solvent (toluene) in the presence of p-toluene sulfonic acid monohydrate. The yield of the di-p-toluene sulfonic acid salt monomer was relatively high (90%) Fig. (1-a).

3.2. Synthesis of poly(ester-amide) based on L-arginine

The Di-p-toluene sulfonic acid salts of O, O′-bis-(L-arginine ester)-cis/*trans*-1,4-cyclohexane monomer and terephthaloyl chloride are polymerized together using an interfacial polycondensation method. First, the prepared monomer was dissolved in water with an inorganic base (KOH), and terephthaloyl chloride was dissolved in the $CHCl_3$. The reaction needed vigorous stirring to increase the surface area available for the reaction to enable the formation of fine polymer particles. The intrinsic viscosities of the prepared poly(ester-amide) were calculated from the viscosity measurements of the dilute polymer solutions (0.5 g/dL) in DMSO at 25 °C. As a result, the polymer has intrinsic viscosity (0.342 ± 0.014 dL/g) and MW 34,200 g/mol. Fig. 1-b [51].

3.3. Synthesis of poly(ester-amide) carbamazepine formula [(CBZ/Arg-PEA) NCs]

CBZ-loaded nanocapsules was created using a simple, safe, and repeatable interfacial polycondensation. It is a condensation reaction between the water phase containing the Di-p-toluene sulfonic acid salts of O, O′-bis-(L-arginine ester)-cis/*trans*-1,4- cyclohexane monomer. The other phase consists of terephthaloyl chloride and CBZ in chloroform

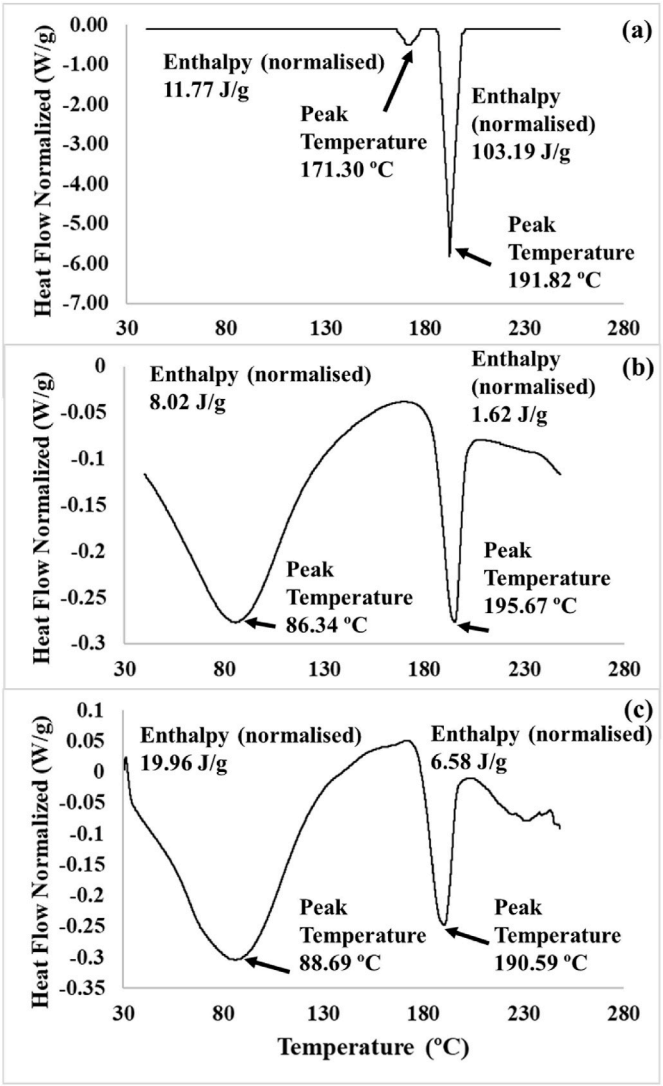

Fig. 4. DSc thermograms for (a) CBZ (b) Arg-PEA and (c) CBZ/Arg-PEA) NCs.

($CHCl_3$). Using this method, direct encapsulation of CBZ resulted in capsules with an average diameter around 400 nm and high-efficiency drug loading of 19.8% [52].

3.4. FTIR spectra analysis

The FTIR spectra of the prepared monomer (Arg-PEA), and (CBZ/Arg-PEA) NCs showed distinct absorption bands for all organic functional groups. However, the prepared monomer showed a strong absorption band due to the carbonyl carbon stretching vibration of the ester at 1697 cm^{-1}. On the other hand, the FTIR spectra of (Arg-PEA) and (CBZ/Arg-PEA) NCs showed the same characteristic bands. They showed strong absorption bands due to the carbonyl stretching vibration of the amide group around 1631cm-^{1}, proving the (Arg-PEA) and (CBZ/Arg-PEA) NCs. Moreover, characteristic absorption bands were observed around 1693 cm^{-1} assigned for the carbonyl ester groups, as shown in Fig. 2. Similar results were reported in our previous work [53–55].

3.5. NMR spectra analysis

^{1}H NMR and ^{13}C NMR characterised the synthesised di-p-toluene sulfonic acid salt of O,O′-bis-(L-arginine ester)- 1,4-cyclohexane monomer and poly(ester-amide) based on L-arginine. The spectra exhibited characteristic chemical shifts corresponding to the different atoms present in the samples. The ^{1}H NMR spectrum of the synthesised monomer confirmed its proposed structure. A pair of doublets appeared at 7.09 and 7.46 ppm that were assigned to protons of the aromatic ring of p-toluene sulfonic acid salt. The signal for the protons of the methyl group attached to the aromatic ring (Ar-CH_3) appeared as a singlet at 2.25 ppm. The signals of 1,4-cyclohexane protons appeared at 3.29 for CH and at 2.45 ppm for CH_2 Fig. (3-a). The protons of the carbons in the arginine were observed for CH at 3.03 ppm and for $3CH_2$ in the range 1.50–1.61 as multiplet. On the other hand, the ^{1}H NMR spectrum confirmed the poly(ester-amide) structure by the appearance of the protons of the terephthaloyl unit that appeared in the aromatic region at 7.64 ppm Fig. (3-b).

The structure of the monomer was also confirmed by ^{13}C NMR spectroscopy. The chemical shift of the formed ester carbonyl carbon is of special importance; it appeared at around 173.3 ppm. The CH and CH_2 carbon peaks were observed in the 68.7 and 33.5 ppm assigned to 1,4-cyclohexane carbons. The aromatic carbons of the p-toluene sulfonic acid salt were observed at 138.6, 128.9, 125.8, and 145.4 ppm. The carbons of the arginine side chain were observed at 54.1, 25.2, 28.8, and 40.7 ppm Fig. (3-c).

Alternatively, the structure of the poly(ester-amide) was also confirmed by ^{13}C NMR. The chemical shift of the formed amide carbonyl carbon atom appeared at 165.2 ppm, and the ester appeared at 177.2 ppm. The carbons of 1,4-cyclohexane were observed at 34.8 ppm for CH_2 and 70.2 ppm for CH. The CH carbon signals of the aromatic rings of the terephthalate unit were observed at 128.7 ppm. The aromatic quaternary carbon of the same unit was observed in the chemical shift at 136.3 ppm Fig. (2-d).

3.6. DSC analysis

CBZ had a melting point that ranges between 189 and 192 °C [38]. However, CBZ is present in different polymorphic forms. The DSC of CBZ alone as can be seen in Fig. 4-a showed a small characteristic endothermic peak at 171.30 °C and a second large peak at 191.82 °C indicating form III. The first peak is based on form III melting followed by crystallisation and melting at a temperature that ranges between 189 and 193 °C [56]. The DSC thermograms for (Arg-PEA) and (CBZ/Arg--PEA) NCs loaded particles are highlighted in Fig. 4-b and c respectively. The polymer is expected to be semi-crystalline, with a glass transition at around 86 °C and a sharp endothermic peak at 195.67 °C Fig. 4-b. However, upon the addition of CBZ to the polymer using interfacial polycondensation, it is expected that the drug will be incorporated within the chains of the polymer. Hence, the DSC showed a wider and higher enthalpy at the glass transition Fig. 4-a [57]. However, some of the drug particles could be attracted to the surface of the polymer and hence a slight shift of the peak at 195 to 190.59, which could be contributed to the presence of CBZ.

3.7. SEM and TEM analysis

SEM images of the (CBZ/Arg-PEA) NCs as depicted in Fig. 5. showed microscale irregular, dense, nanoaggregates. In Fig. (5-C), it was clear that the particles are within submicron size (below 1 μm), in line with the results obtained from the zeta sizer. Furthermore, submicron agglomerates were connected at higher magnifications to form larger micron-sized particles, enabling their administration into the nasal cavity. A study reported that powders with very small particle sizes tend to deposit at the entry of the nostrils and hence will not reach the brain [32]. Further, micron size aggregates enhanced the flowability of the powder upon intranasal inhalation. However, the images showed some artifacts which is attributed to the sample preparation method and positioning errors [58]. TEM images when compared to SEMs (see Fig. 5D–F) generated higher-resolution images and was able to deliver information regarding individual nanoparticle, which allowed to explore further inner properties of the sample [59]. TEM analysis was

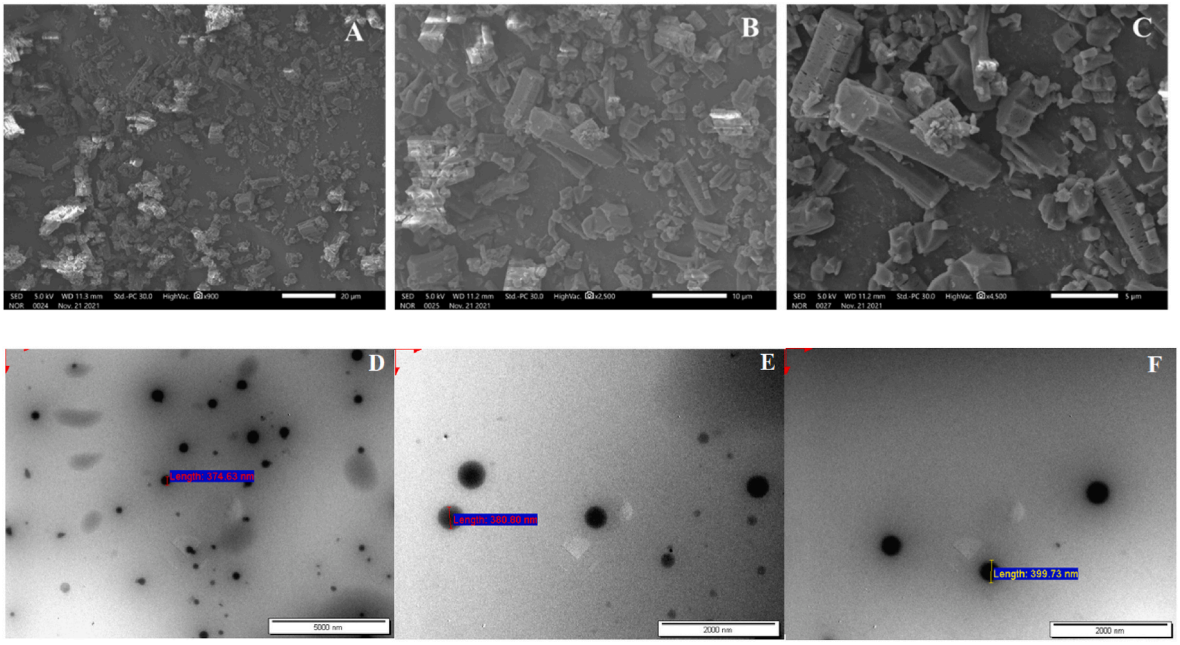

Fig. 5. SEM images of (CBZ/Arg-PEA) NCs at various magnifications (A) 900 (B) 2400 and (C) 4500 (D–F) TEM analysis of (CBZ/Arg-PEA) NCs.

carried out to find the shape and size of the nanoparticles. Fig. (5-D, E&F) indicated TEM images of (CBZ/Arg-PEA) NCs. From TEM, the nanoparticles are observed to have a roughly spherical shape with size range between 372 and 499 nm.

3.8. XRD analysis

CBZ is a crystalline material, and based on literature, it has several characteristic intense peaks such as at [39]. The XRD patterns of CBZ (Fig. 6-a) showed database matches for CBZ which correspond to mainly form III. Key characteristic peaks for CBZ Form III can be seen in strong peaks at $2\theta = 15.21$, 20.03, 24.80 and 27.20. These results are in agreement with a reported data [56]. The XRD patterns of Arg-PEA and the (CBZ/Arg-PEA) NCs are depicted in Fig. (6-b) and Fig. (6-c), respectively. The (Arg-PEA) diffractograms showed a typical semi crystalline substance, with several intense peaks in their diffractograms between $2\theta = 20\text{-}30^{\circ}$. However, it was noted that the (CBZ/Arg-PEA) NCs samples showed a similar pattern to that of the polymer alone. The absence of characteristic crystal peaks of CBZ in the diffractograms of formulation (F8) Fig. (6-a) suggest that CBZ was dispersed in the semi-crystalline form of the polymer [60].

3.9. Quality by design analysis (QbD)

Optimisation to produce (CBZ/Arg-PEA) NCs was carried out using QbD. A total of 17 runs were generated by MODDE software which was prepared and characterised depending on the proposed run order. Table 4 denotes the CCF design worksheet with the quantities of input parameters, CQA results, the total number of runs, and the run order. The results were fitted to the MODDE software to enable analysis.

The fitted data were represented in the summary of the fit plot (see Fig. 7.) after the exclusion of 3 experiments (N3, N9, and N12) to enhance the model validity and prediction power. From the graph, the first bar of each response (the bright green bar) represented R2 and is assigned to the degree of fitting of the data to the model, where the greater the R2 the more the data is fitted to the model (preferably >0.5). From the plot, R2 was exceeded 0.9 for all the responses indicating an excellent fit of the data into the model (values exceeded 0.9). The second bar (dark-blue bar) represented the ability of the model to precisely predict future data (denoted by Q2). For each response, a Q2 value exceeding 0.5 is a good model regarding predictability. As can be seen from the graph, none of the responses were below the threshold mark of 0.5. Hence, the prediction power of the model was good. Furthermore, the third bar represented the model validity, which needs to exceed 0.25. Once the model outliners were excluded, the validity for all responses was above 0.25. The final bar represented reproducibility. However, concerning reproducibility, all models were considered reproducible. Which means that replicates present in runs comparatively give the identical response. Consequently, the overall model was fit and ready for further verification processes.

3.9.1. Model verification

Model verification was continued by assessing model terms in which insignificant model terms were excluded. The final model was fitted with eight model terms namely: a constant, single model terms (API, AQU, ORG), the quadratic model term (API*API, AQU*AQU, ORG*ORG) while only one interactive term was significant (API*AQU).

Further validation tools were used, such as the normal probability plot of residuals that were plotted as can be noted in Fig. (8-a). This plot is valuable to identify any outlier experiments and the normality of the residual model. From the figure, the residuals in the four responses were within the acceptable range of ±4 standardized residuals and hence no outliers can be noted. In this model, all the residuals were within ±2 standardized residuals.

Assessing the relationship between observed values versus predicted values for each response as shown in Fig. (8-b) was conducted. As can be seen from the graph, all responses showed an excellent correlation between observed and predicted values. The results indicated linear correlation with high regression coefficient for PSA (0.9866), EE (0.991), ENC (0.9737), and % release after 24 h (0.9409) which suggested an excellent model. The final verification tool was the plot of residues versus run order. The value of this plot is to show if the error is built up with the run order. A valid model is when the error is randomly distributed as can be seen in Fig. (8-c).

3.9.2. Analysis of variance (ANOVA) results

Results of ANOVA analysis are summarized in Table 5. The results showed that the regression model for all the responses was significant (p-value <0.05) whereas, the significance that could be attributed to error or lack of fit was not significant (p-value >0.05). Hence this model

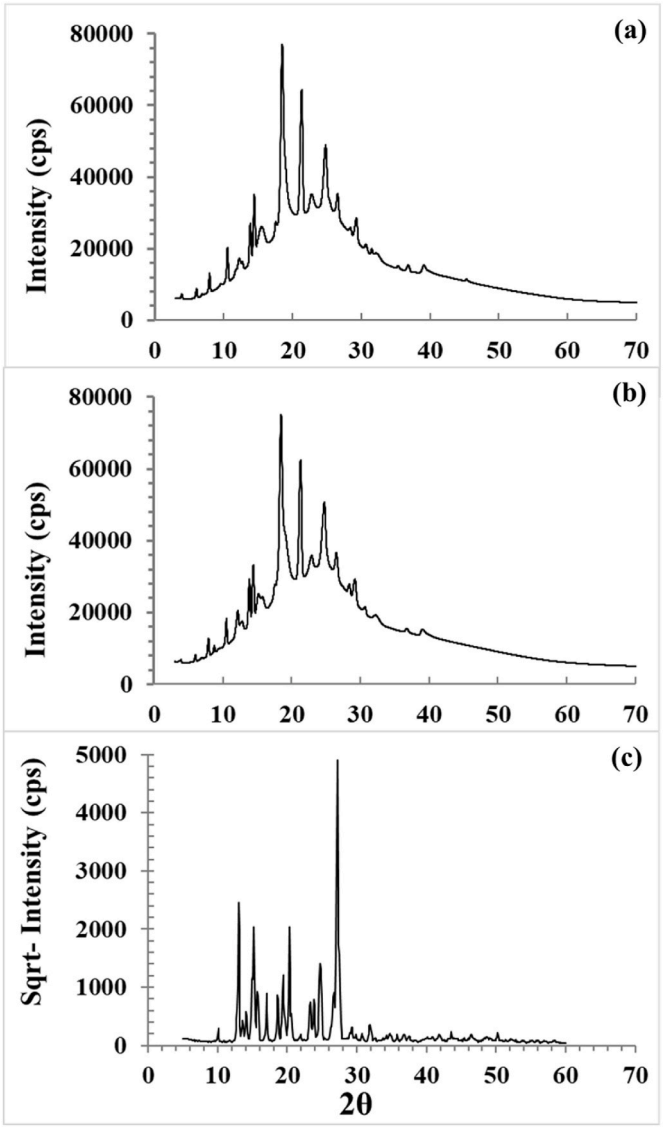

Fig. 6. XRD pattern for (a) Arg-PEA and (b) the (CBZ/Arg-PEA) NCs and (c) CBZ.

is statistically valid.

3.9.3. Regression model equations

Once the model demonstrated validity and significance, the regression model equations for all the responses were identified. Using the regression coefficient plot as can be seen in Fig. (8-d) the significant model terms for each response were evaluated and if significant were included in the regression equation. The bar length indicates the magnitude of the effect of the model term on the response, while its direction suggests whether its effect was positive or negative on the response. Nevertheless, the error bars explain the significance of each model term. If the error bar crosses the zero line, the corresponding term is deemed as nonsignificant. Therefore, the regression model equation for each response entails only the significant terms. For example, for particle size the most significant term was the quadratic term API*API, with a positive effect, i.e., increasing the CBZ concertation at the very beginning from low to moderate results in a reduction in particle size while if it increases after a certain limit, the effect is reversed, and larger particles are produced. Because in our study the polymer is more hydrophilic, and this means that it is favouring the aqueous phase so a higher volume of the aqueous phase leads to a higher degree of dispersion so a smaller particle size could be obtained. Additionally, as can be seen from Fig. (8-d), the volume of the aqueous phase had a key effect on all responses.

The regression equations for all the responses are depicted in the following equations:

$$Y_1 = 298.3 - 18.5\,X_1 - 45.2\,X_2 + 60.1X_1^2 + 36.5\,X_2^2 - 70.8X_1X_2 \quad \text{Eq (3)}$$

$$Y_2 = 99.1 + 1.3X_1 + 3.2X_2 + 0.73X_3 - 2.8X_1^2 - 3.1\,X_3^2 + 1.0\,X_1X_2 \quad \text{Eq (4)}$$

$$Y_3 = 21.8 + 1.3X_1 + 3.0X_2 - 2.8X_1^2 - 2.8\,X_3^2 + 1.7\,X_1X_2 \quad \text{Eq (5)}$$

$$Y_4 = 88.7 + 2.6X_2 - 4.7X_1^2 + 5.3\,X_1X_2 \quad \text{Eq (6)}$$

where (Y_1) is the particle size of the nanocapsules, (Y_2) is the entrapment efficiency, (Y_3) is the loading efficiency, and (Y_4) is the percentage released of the CBZ after 24 h. As for the factors, (X_1) stands for CBZ concentration (%), (X_2) represents aqueous phase volume (mL), and (X_3) is the organic phase volume (mL). Like the main effect graphs, the value of each coefficient assigned for its impact and its sign indicates the positivity or negativity of the effect on the response. For example, the most significant effect on % release was the interactive term (+5.3 X_1*X_2) having a vital positive effect on the degree of release of the CBZ.

Table 4
The CCF design worksheet with the factors, responses, results, the total number of runs and the run order.

Exp No	Exp Name	Run Order	Incl/Excl[a]	API	AQU VOL	ORGA VOL	%EE	%ENCE	PSA	%RELEASE
1	N1	12	Incl	−1	−1	−1	83.1	6.6	480	81
2	N2	3	Incl	1	−1	−1	84.4	7.4	560	72
3	N3	9	Excl	−1	1	−1	95.2	11.8	265	91
4	N4	4	Incl	1	1	−1	94.5	17.1	260	89
5	N5	5	Incl	−1	−1	1	83.6	6.9	500	79
6	N6	14	Incl	1	−1	1	87.9	7.1	550	70
7	N7	8	Incl	−1	1	1	88.5	7.5	693	65
8	N8	11	Incl	1	1	1	98.5	20.8	290	92
9	N9	10	Excl	−1	0	0	89.8	9.5	300	90
10	N10	15	Incl	1	0	0	97.6	19.2	350	86
11	N11	13	Incl	0	−1	0	94.4	17.1	370	85
12	N12	17	Excl	0	1	0	92.4	14.5	280	94
13	N13	1	Incl	0	0	−1	93	15	300	93
14	N14	2	Incl	0	0	1	96.1	18.2	310	92
15	N15	16	Incl	0	0	0	99.6	23.5	310	88
16	N16	7	Incl	0	0	0	99	21.6	320	85
17	N17	6	Incl	0	0	0	99.2	22.6	306	86

[a] Incl: the run was included in the analysis; Excl: the run was excluded from the analysis (outlier). API is the amount of CBZ.

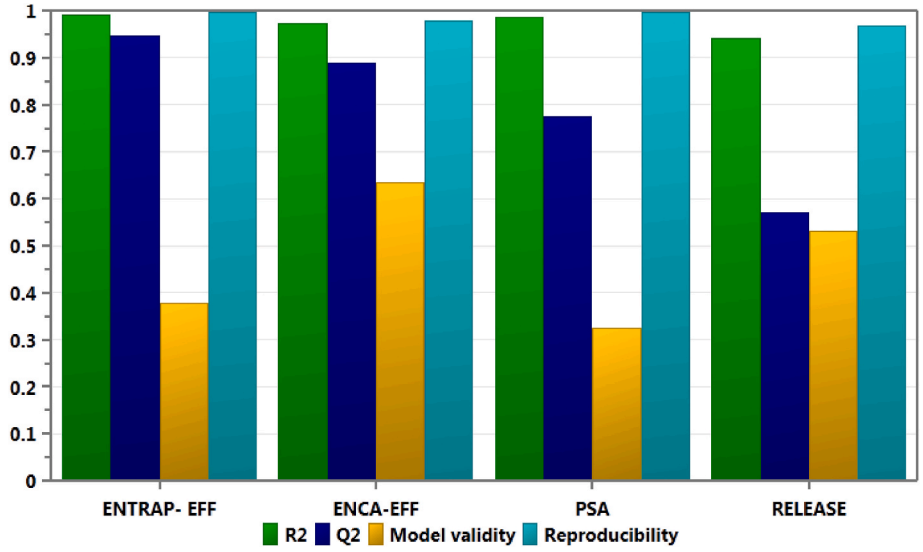

Fig. 7. Summary plot of the four responses (CQA) of fit showing model fit (R2), predictability (Q2), model validity and reproducibility. ENTRAP-EFF: entrapment efficiency; ENCA-EFF: loading efficiency; PSA: particle size; Release is % released of CBZ after 24 h.

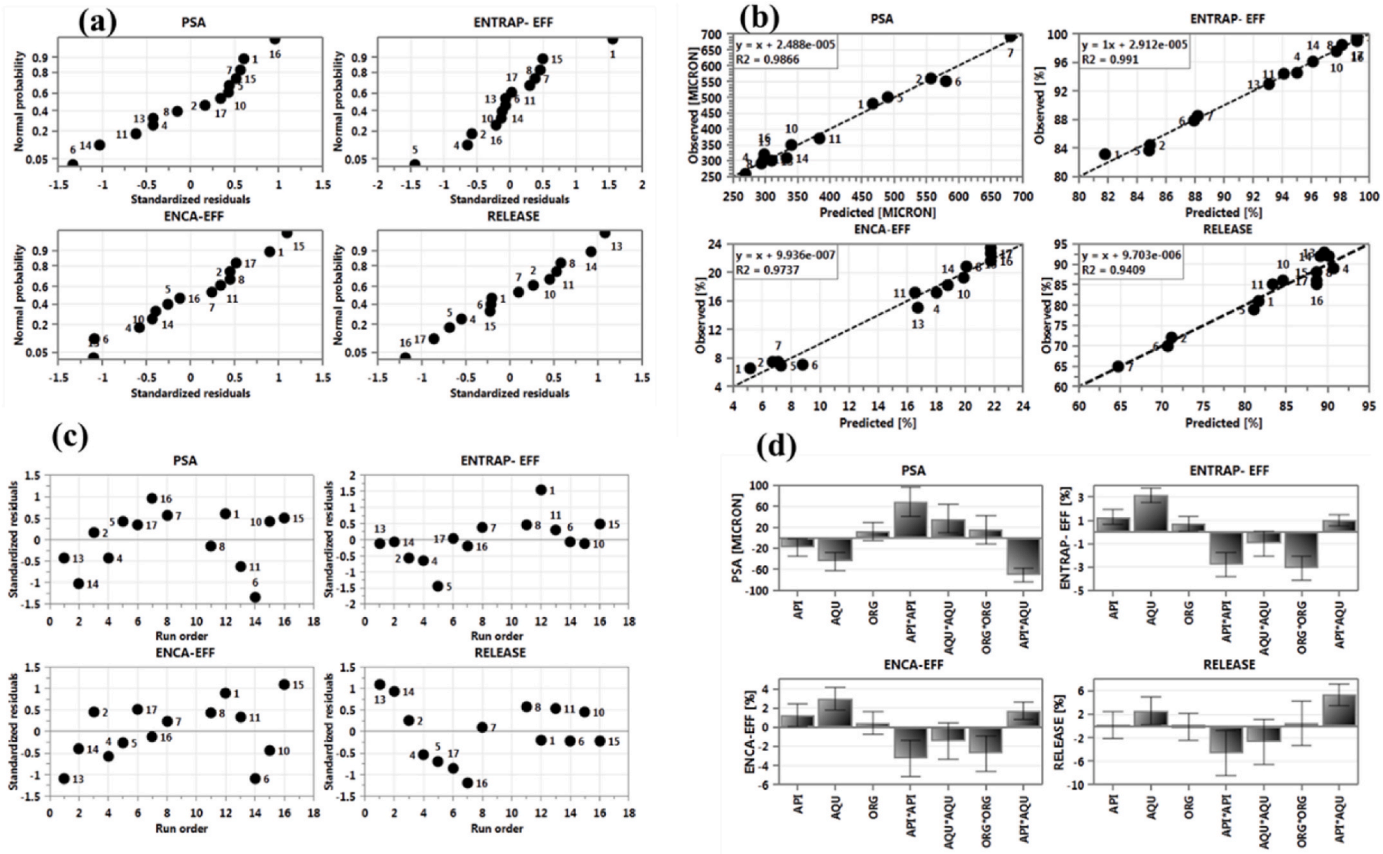

Fig. 8. Model validation plots (a) the normal probability plot of residuals showing that all responses are normally distributed and there is no outlying runs (within the range −4 to +4 SD); (b) The observed values versus the predicted ones for all the responses that highlight the correlation of predicted values with observed values; (c) the residual versus run order for all responses highlighting the randomness of residual within runs and hence a good and valid model; (d) regression coefficients plot of the seven model terms for each response highlighting the magnitude, direction, and significance of each term for each response.

3.9.4. Effect of critical input parameters on responses

The following section will discuss the effect of various factors on each response with emphasis on significant single, quadratic, and interactive effects. The main single factor affecting all the responses is the concertation of the CBZ (Fig. 9). Increasing the CBZ concertation resulted in a reduction in the particle size of the nanoparticles, when the CBZ concertation is between the low and medium range, whereas, when the CBZ concertation tends to go up to the higher range may result in a constant and or slight increase in the particle size. This could be attributed to the ability of the amount of solvent used to dissolve the CBZ

Table 5
Summary of the results obtained from ANOVA for the four responses.

Response	P	R2
Particle Size		
Regression	0.000	0.987
Lack to fit	0.067	
Entrapment Efficiency		
Regression	0.000	0.991
Lack to fit	0.083	
Loading Efficiency		
Regression	0.000	0.974
Lack to fit	0.232	
% Release		
Regression	0.003	0.941
Lack to fit	0.154	
Lack to fit	0.749	

when reaches equilibrium this will lead to particle size aggregate and hence larger particle size. However, as can be seen from equation (3), the CBZ demonstrated a quadratic positive effect. Such effect can be presented as a convex curve [31]. Such a curve could be divided into two sections, the first is the descending part were increasing the CBZ concentration will result in a reduction in particle size, a concertation above the middle one increased the particle size as discussed earlier.

Although increasing the CBZ concertation enhanced entrapment efficiency, the entrapment of the CBZ exceeded 90% at all CBZ ranges. Further, the loading efficiency of the CBZ demonstrated an increase when the CBZ concertation increases from low to medium range. Higher amounts of the CBZ did not result in a steady increase in the loading efficiency. Further, the CBZ concertation did not alter the release of the drug.

Fig. 10 shows the effect of aqueous phase volume on the four responses. Apart from its effect on particle size, increasing the AQU VOL resulted in enhancement of entrapment efficiency, loading efficiency, and % release of the CBZ. This could be attributed to the concept of smaller particle size leads to higher surface area and so more surfaces will be in contact with the environment and hence release will be enhanced. The increase in AQU VOL resulted in a reduction of the size of the nanoparticles because the polymer seems to favour the aqueous medium to disperse in it.

Fig. 11 highlighted the interactive effect of the concentration of the CBZ and the AQU VOL on the particle size of the nanoparticles. Low CBZ concentration, low AQU VOL will give larger particles, while increasing the CBZ concentration and AQU VOL a reduction of the particle size is observed. This could be justified that even if the amount of CBZ increased it would give a smaller particle size when they found enough amount of aqueous phase. Therefore, using a high concentration of the CBZ and aqueous phase will give the best nanoparticles.

Similarly, Fig. 12 shows the effect of CBZ concentration and aqueous phase volume on all the responses. Using higher CBZ concentration requires high aqueous volume to reduce the particle size, whereas, at lower CBZ concentration, the effect of aqueous volume is minimized. From the graph, both entrapment efficiency and loading efficiency work better at higher aqueous volume particularly when the CBZ concentration increased. The extended-release behaviour was observed with low CBZ concentration particularly when the aqueous volume is large. This could be attributed to the slightly larger particles.

Overall, the effect of organic phase volume was not significant for particle size and the release profile of the particles. This insignificant effect could be explained as that one of the phases will show a significant effect mainly on the particle size and here as discussed earlier the polymer tend to be in the aqueous phase more than the organic phase because of the NH^{+} charge that is present already in arginine structure. While increasing, it resulted in a slight reduction of both entrapment efficiency and loading efficiency as can be seen in Equations (2) and (3).

3.9.5. *Prediction of the design space*

Employing the results obtained from individual and interactive effects on the responses, the best area in which all the results of the responses are within the desired range such as, low particle size (200–400 nm), high entrapment efficiency (80–100%), loading efficiency (15–30%) and targeted release (60–80% after 24 h). Organic phase was kept at medium volume. According to the sweet spot plot of Fig. 13, the red coloured areas represent the design space in which all the responses results were within the targeted values. While other colours correspond to areas where factors would meet the specification of three, two, or one

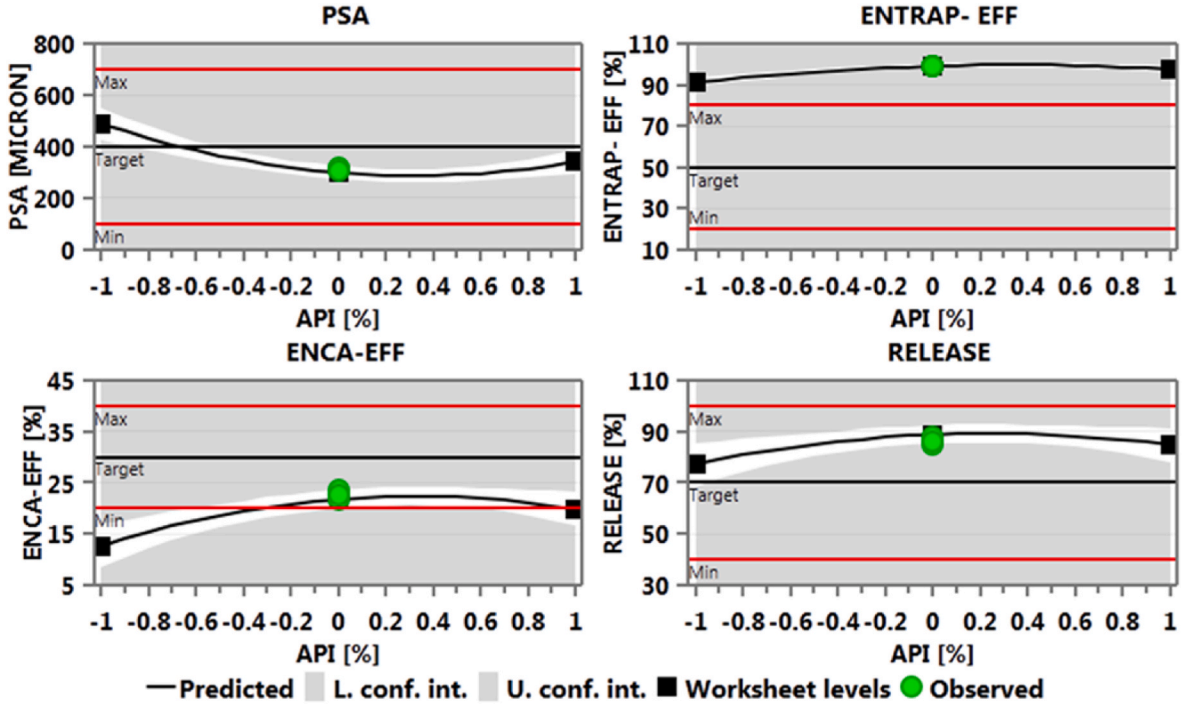

Fig. 9. The effect of CBZ concentration on all responses.

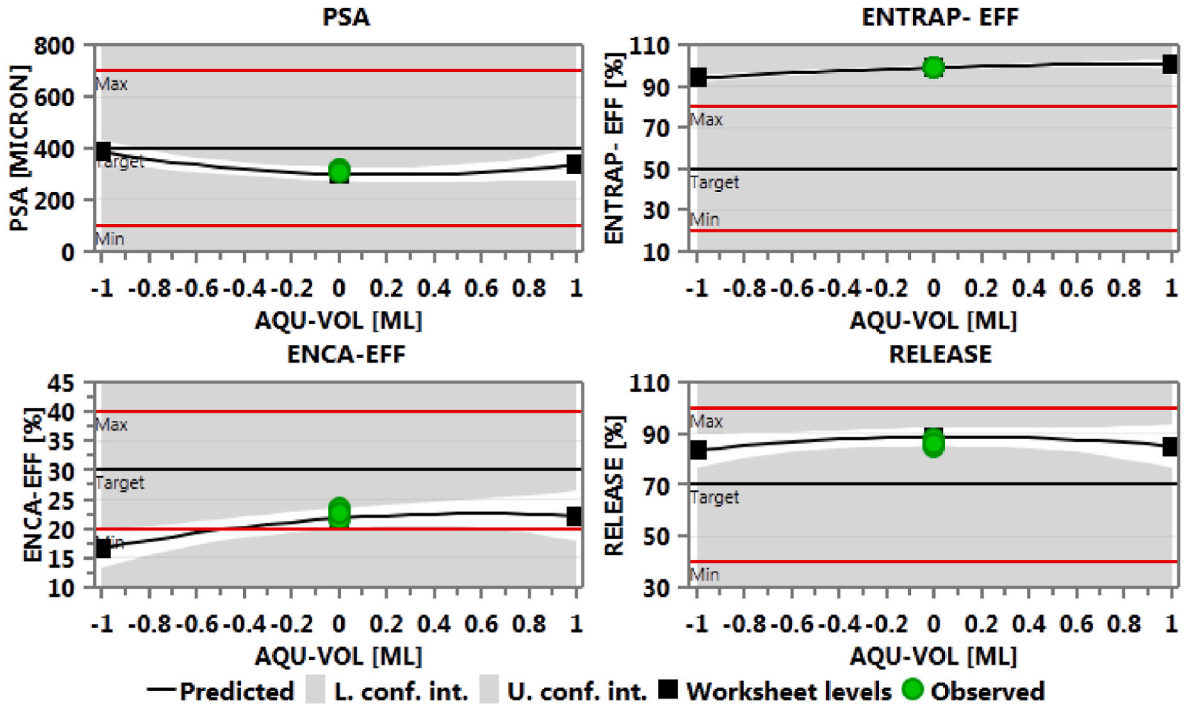

Fig. 10. The effect of the aqueous phase volume on all responses.

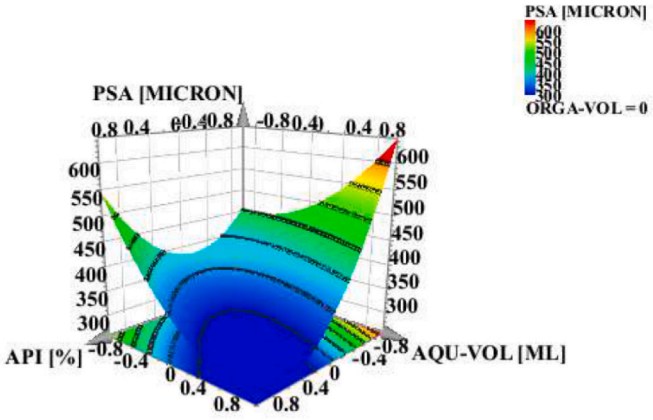

Fig. 11. RSM of the interactive effect of CBZ concentration and AQU-VOL on the particle size of the nanoparticles.

response. Two points were selected to represent optimal formulations. In point A see Fig. 13 when (−0.332, 240 mg) CBZ concentration is prepared with the highest volume of aqueous phase while the organic phase is kept at its medium range, a formulation will be produced with particle size of 411 nm, entrapment efficiency of 98.9%, loading efficiency 19.8% and a release after 24 h reaching 79%. In another example (point B), maximum CBZ concentration is prepared with the (−0.34) of aqueous phase while the organic phase is kept at its medium range, a formulation will be produced with particle size of 405 nm, entrapment efficiency of 95.5%, loading efficiency 17.8% and a release wafter 24 h reaching 80%.

3.10. In vivo study

Fig. 14 presents the data obtained from HPLC brain analysis, revealing the capability of nose-brain treatment with nanocapsules (NCs) to deliver CBZ directly to the brain. The results demonstrate a sustained increase in brain concentration at 2, 5, and 10 min after treatment, indicating both an initial burst effect, representing the release of CBZ attached to the polymer surface, and subsequent degradation of the polymer chain, leading to the release of CBZ from the inner core. These findings suggest that CBZ can reach the brain through olfactory and trigeminal pathways, bypassing the first-pass metabolism of the gastrointestinal tract and liver.

Fig. 15 depicts the anticonvulsant evaluation using PTZ, demonstrating that intranasal administration of (CBZ/Arg-PEA) NCs significantly increased seizure onset time and reduced seizure duration and scores compared to oral CBZ. These findings highlight the potent anticonvulsant properties of (CBZ/Arg-PEA) NCs, demonstrating their ability to effectively mitigate seizure activity. While their efficacy was lower than orally administered DZP, our results provide compelling evidence for the potential of intranasal nanocapsule delivery as a valuable therapeutic approach for managing seizures, offering rapid and targeted anticonvulsant effects. Further optimisation of (CBZ/Arg-PEA) NCs may enhance their effectiveness, potentially rivalling standard anticonvulsant medications. This study emphasized the promising role of intranasal NCs as a novel and effective route for anticonvulsant drug delivery. Additionally, a previous study's demonstration of carboxymethyl chitosan nanoparticles' efficacy in delivering CBZ intra-nasally [42] supports our investigation of (CBZ/Arg-PEA)NCs via the same route, indicating enhanced brain targeting and drug bioavailability.

Based on the findings of this study, it is recommended to conduct an analysis of plasma kinetics to further investigate the pharmacokinetics of CBZ following intranasal administration using NCs. Conducting an analysis of plasma kinetics would provide important insights into the systemic pharmacokinetics of CBZ delivered intranasally using nanocapsules. This information would enhance our understanding of the drug's absorption, distribution, metabolism, and elimination, and contribute to the optimisation and development of intranasal delivery systems for improved anticonvulsant therapy.

4. Conclusions

In the present study, nanocapsules poly(ester-amide) based on the L-arginine amino acid loaded with carbamazepine was successfully

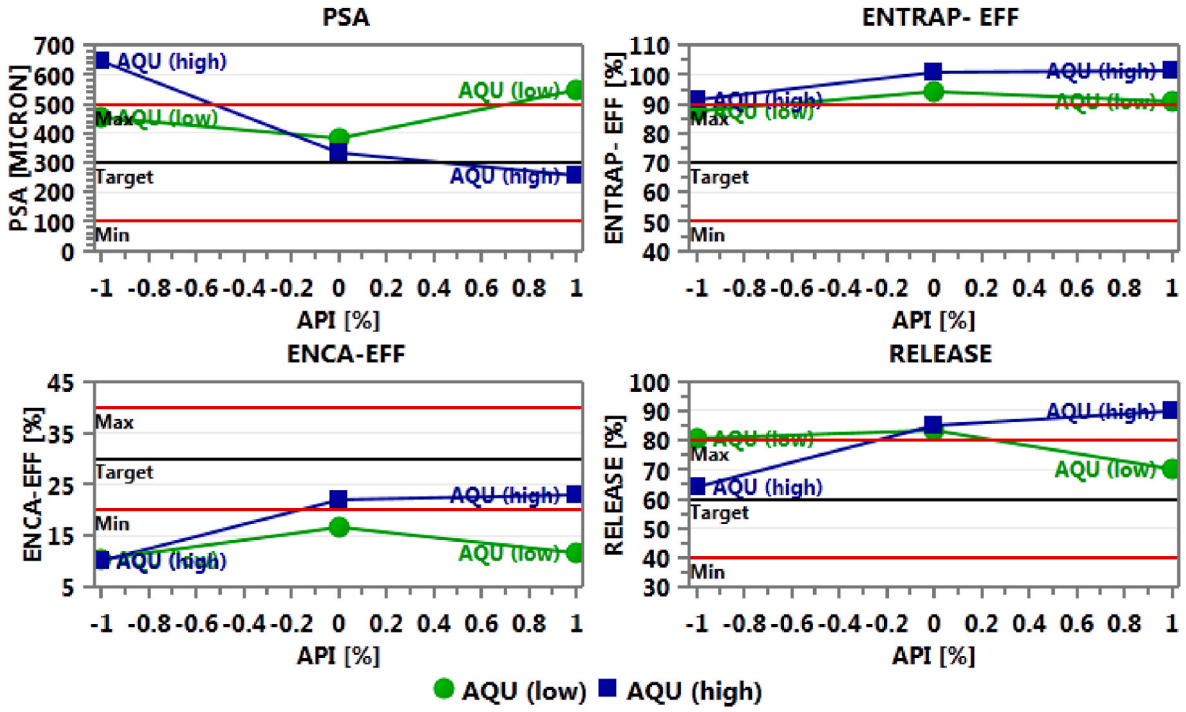

Fig. 12. The interactive effect of CBZ concentration and AQU-VOL on all responses.

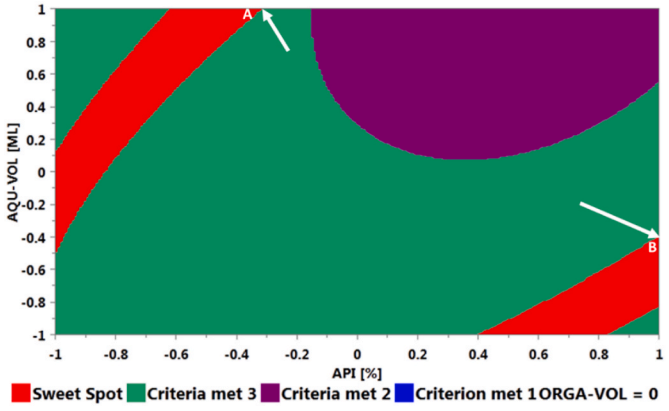

Fig. 13. The sweet spot for optimal proportion ranking of factors (CBZ concentration, Aqueous phase volume to obtain the desired response values relating to low particle size (200–400 nm), high entrapment efficiency (80–100%) and loading efficiency (15–30%) and targeted release (40–80% after 24 h. The organic phase was kept at medium volume. Selected formulations are (A) and (B).

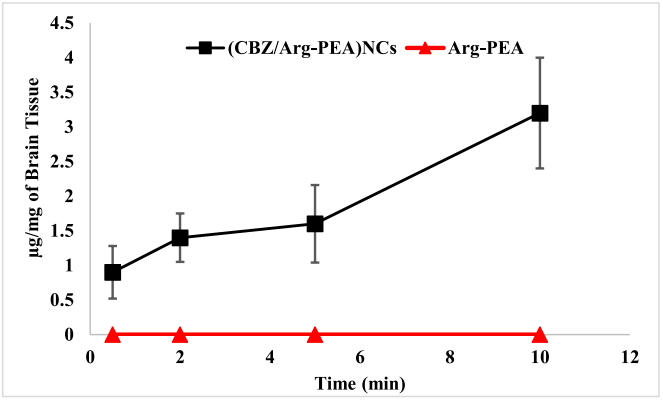

Fig. 14. Amount of CBZ in the brains of mice sacrificed immediately (at time 0.5 min) and at 2, 5, and 10 min after intranasal treatment with (CBZ/Arg-PEA) NCs.

synthesised and further optimised using the interfacial polycondensation method. Quality by design method was employed to determine the best process parameters to produce formula with favourable attributes according to three critical factors: carbamazepine concentration, aqueous phase volume, and organic phase volume. The results of this project revealed that using a high concentration of carbamazepine and aqueous phase will produce the optimal nanoparticles in terms of lower particle size, higher entrapment efficiency, loading efficiency and extended the release of the CBZ after 24 h. In comparison, the effect of organic phase volume was not significant for particle size and the release profile of the particles. Animal studies were also done to prove the ability of poly(ester-amide) nanocapsules to be used as a carrier for CBZ directly from the nose to the brain. Results show excellent ability to reach the brain even with a very fast onset of action. This result can be a sign of success to approve the idea of this study, and it could be a blueprint in biopharmaceutical science because it will be the beginning of a new dosage form of CBZ.

Ethics approval and consent to participate

Approval was granted by the Scientific Research Ethics Committee of Isra university (SREC/23-19/2020/2021).

Consent for publication

This study does not involve human subjects.

Availability of data and materials

All data generated or analysed during this study are included in this published article.

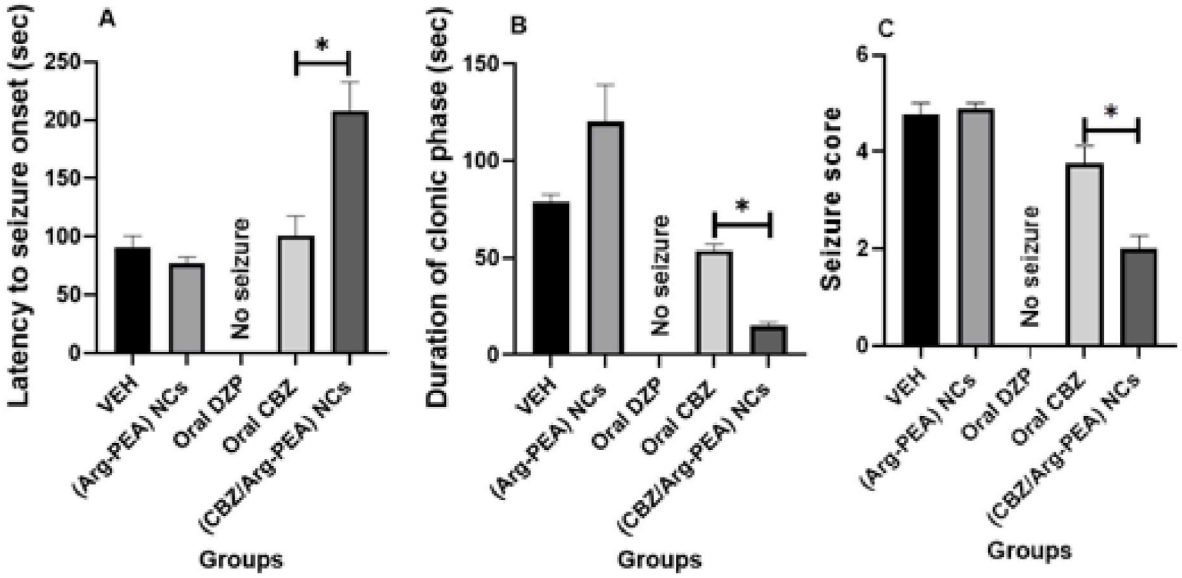

Fig. 15. Anticonvulsant effect of (CBZ/Arg-PEA) NCs against seizure induced by intraperitoneal administration of PTZ at a dose of 80 mg/kg in mice. The bar graphs depict the mean ± SEM of various analysed parameters, with a sample size of 8 mice per group. (A) The graph illustrates the impact of (CBZ/Arg-PEA) NCs on the latency to seizure onset. Significant differences (denoted by *) were observed between CBZ/Arg-PEA and oral CBZ groups at a significance level of $P < 0.0001$ (B) The graph represents the influence of CBZ/Arg-PEA on the duration of seizures. Significant differences (denoted by *) were observed between (CBZ/Arg-PEA)NCs and oral CBZ groups at a significance level of $P < 0.05$ (C) The graph demonstrates the effect of CBZ/Arg-PEA on the seizure score. The statistical analysis involved using ANOVA followed by Tukey's test. Significant differences (denoted by *) were observed between (CBZ/Arg-PEA) NCs and oral CBZ groups at a significance level of $P < 0.0001$.

Funding

Isra University (Jordan) was funding Dr. Dalia Ali (grant 23-19/2020/2021).

Authors' contributions

Noor Mohammed Al-Baldawi: investigation; data curation; formal analysis. Dalia Khalil Ali: conceptualisation; writing–review & editing; supervision; project administration; funding acquisition. Eman Zmaily Dahmash: conceptualisations; writing – review & editing; supervision; project administration. Qais Jarrar: investigation; data curation; formal analysis; review & editing supervision; Rasha Abuthawabeh: investigation.

Declaration of competing interest

The authors declare that they have no known competing financial interests or personal relationships that could have appeared to influence the work reported in this paper.

Data availability

Data will be made available on request.

Acknowledgments

The authors acknowledge the support of Isra University (Jordan) for funding Dr. Dalia Ali (grant 23-19/2020/2021). Also, the authors further acknowledge Kingston University for supporting Dr. Eman Dahmash.

Appendix A. Supplementary data

Supplementary data to this article can be found online at https://doi.org/10.1016/j.jddst.2023.105070.

References

[1] R.T. Branquinho, et al., Biodegradable polymeric nanocapsules prevent cardiotoxicity of anti-trypanosomal lychnopholide, Sci. Rep. 7 (1) (2017) 1–13.
[2] S. Deng, M.R. Gigliobianco, R. Censi, P. Di Martino, Polymeric nanocapsules as nanotechnological alternative for drug delivery system: current status, challenges and opportunities, Nanomaterials 10 (5) (2020) 847.
[3] N.M. Alkurdi, S.H. Hussein-al-ali, A. Albalwi, M.K. Haddad, Y. Aldalahmed, D. K. Ali, Development and Evaluation of a Novel Polymer Drug Delivery System Using Cromolyn-Polyamides-Disulfide Using Response Surface Design, vol. 2022, 2022.
[4] Z.A.G. Ahmed, et al., Development and evaluation of amlodipine-polymer nanocomposites using response surface methodology, Int. J. Polym. Sci. 2022 (2022), https://doi.org/10.1155/2022/3427400.
[5] D.K. Ali, S.H. Al-Ali, E.Z. Dahmash, G. Edris, H.S. Alyami, Reduction and pH dualresponsive biobased poly(disulfide-amide) nanoparticles using cystine amino acid for targeting release of doxorubicin anticancer drug, J. Polym. Environ. (2022), https://doi.org/10.1007/s10924-022-02552-9.
[6] V. Marturano, V. Ambrogi, P. Cerruti, M. Giamberini, B. Tylkowski, Photo-triggered release in polyamide nanosized capsules, AIP Conf. Proc. 1599 (2014) 234–237, https://doi.org/10.1063/1.4876821.
[7] U. Bazylińska, et al., Polymeric nanocapsules with up-converting nanocrystals cargo make ideal fluorescent bioprobes, Sci. Rep. 6 (1) (2016) 1–14.
[8] P. Kothamasu, H. Kanumur, N. Ravur, C. Maddu, R. Parasuramrajam, Nanocapsules : the Weapons for Novel Drug Delivery Systems, vol. 2, 2012, pp. 71–81, https://doi.org/10.5681/bi.2012.011, 2.
[9] K. Landfester, V. Maila, Nanocapsules with Specific Targeting and Release Properties Using Miniemulsion Polymerization, 2013, pp. 1–17.
[10] K. Kamburova, K. Mitarova, T. Radeva, Polysaccharide-based nanocapsules for controlled release of indomethacin, Colloids Surfaces A Physicochem. Eng. Asp. (2016), https://doi.org/10.1016/j.colsurfa.2016.05.040.
[11] D. Crespy, Advanced Stimuli-Responsive Polymer Nanocapsules with Enhanced Capabilities for Payloads Delivery, vol. 6, 2015, https://doi.org/10.1039/c5py00323g, 23.
[12] R.H. Utama, Y. Jiang, P.B. Zetterlund, M.H. Stenzel, Biocompatible Glycopolymer Nanocapsules via Inverse Miniemulsion Periphery RAFT Polymerization for the Delivery of Gemcitabine, 2015, https://doi.org/10.1021/acs.biomac.5b00545.
[13] K. Landfester, M.S. Alkanawati, C. Marques, V. Maila, Polysaccharide-Based pH-Responsive Nanocapsules Prepared with Bio-Orthogonal Chemistry and Their Use as Responsive Delivery Systems, 2020, https://doi.org/10.1021/acs.biomac.0c00492.
[14] X. Ouyang, et al., Synthesis and characterization of triethylene glycol dimethacrylate nanocapsules used in a self-healing bonding resin, J. Dent. 39 (12) (2011) 825–833, https://doi.org/10.1016/j.jdent.2011.09.001.
[15] A.C. Fonseca, M.H. Gil, P.N. Simões, Biodegradable poly(ester amide)s - a remarkable opportunity for the biomedical area: review on the synthesis,

characterization and applications, Prog. Polym. Sci. 39 (7) (2014) 1291–1311, https://doi.org/10.1016/j.progpolymsci.2013.11.007.
[16] S. Zhang, P. Xin, Q. Ou, G. Hollett, Z. Gu, J. Wu, Poly (ester amide)-based hybrid hydrogels for efficient transdermal insulin delivery, J. Mater. Chem. B 6 (42) (2018) 6723–6730, https://doi.org/10.1039/C8TB01466C [Online]. Available:.
[17] X. Pang, J. Wu, C. Reinhart-King, C.C. Chu, Synthesis and characterization of functionalized water soluble cationic poly(ester amide)s, J. Polym. Sci. Part A Polym. Chem. 48 (17) (2010) 3758–3766, https://doi.org/10.1002/pola.24160.
[18] D. Yamanouchi, J. Wu, A.N. Lazar, K. Craig Kent, C.C. Chu, B. Liu, Biodegradable arginine-based poly(ester-amide)s as non-viral gene delivery reagents, Biomaterials 29 (22) (2008) 3269–3277, https://doi.org/10.1016/j.biomaterials.2008.04.026.
[19] X. You, Z. Gu, J. Huang, Y. Kang, C.-C. Chu, J. Wu, Arginine-based poly (ester amide) nanoparticle platform: from structure–property relationship to nucleic acid delivery, Acta Biomater. 74 (2018) 180–191, https://doi.org/10.1016/j.actbio.2018.05.040 [Online]. Available:.
[20] A.C. Fonseca, et al., Poly(ester amide)s based on (L)-lactic acid oligomers and α-amino acids: influence of the α-amino acid side chain in the poly(ester amide)s properties, J. Biomater. Sci. Polym. Ed. 24 (12) (2013) 1391–1409, https://doi.org/10.1080/09205063.2012.762293.
[21] A.C. Fonseca, J.F.J. Coelho, M.H. Gil, P.N. Simões, Poly(ester amide)s based on l-lactic acid oligomers and glycine: the role of the central unit of the l-lactic acid oligomers and their molecular weight in the poly(ester amide)s properties, Polym. Bull. 71 (12) (2014) 3085–3109, https://doi.org/10.1007/s00289-014-1239-6.
[22] Y. Zhou, Z. Gu, J. Liu, K. Huang, G. Liu, J. Wu, Arginine based poly (ester amide)/hyaluronic acid hybrid hydrogels for bone tissue Engineering, Carbohydr. Polym. 230 (2020), 115640, https://doi.org/10.1016/j.carbpol.2019.115640 [Online]. Available:.
[23] J. Wu, D. Yamanouchi, B. Liu, C.C. Chu, Biodegradable arginine-based poly(ether ester amide)s as a non-viral DNA delivery vector and their structure-function study, J. Mater. Chem. 22 (36) (2012) 18983–18991, https://doi.org/10.1039/c2jm33753c.
[24] A. Rodríguez-Galán, L. Franco, J. Puiggalí, Biodegradable Poly (Ester Amide) S: Synthesis and Applications, 2011.
[25] J. Wu, D. Yamanouchi, B. Liu, C.-C. Chu, Biodegradable arginine-based poly (ether ester amide) s as a non-viral DNA delivery vector and their structure–function study, J. Mater. Chem. 22 (36) (2012) 18983–18991.
[26] J.F. Su, L.X. Wang, L. Ren, Z. Huang, X.W. Meng, Preparation and characterization of polyurethane microcapsules containing n-octadecane with styrene-maleic anhydride as a surfactant by interfacial polycondensation, J. Appl. Polym. Sci. 102 (5) (2006) 4996–5006, https://doi.org/10.1002/app.25001.
[27] L. Torini, J.F. Argillier, N. Zydowicz, Interfacial polycondensation encapsulation in miniemulsion, Macromolecules 38 (8) (2005) 3225–3236, https://doi.org/10.1021/ma047808e.
[28] L. Wang, Y. Wang, D. Cao, Synthesis and characterization of novel biodegradable polyamides containing α-amino acid, J. Macromol. Sci. Part A Pure Appl. Chem. 46 (3) (2009) 312–320, https://doi.org/10.1080/10601320802637441.
[29] B. Begines, F. Zamora, M.V. De Paz, K. Hakkou, J.A. Galbis, Polyurethanes derived from carbohydrates and cystine-based monomers, J. Appl. Polym. Sci. 132 (3) (2015) 1–8, https://doi.org/10.1002/app.41304.
[30] D.K. Ali, A.M. Al-zuheiri, B.A. Sweileh, International Journal of Polymer Analysis and pH and Reduction Sensitive Bio-Based Polyamides Derived from Renewable Dicarboxylic Acid Monomers and Cystine Amino Acid, vol. 5341, 2017, https://doi.org/10.1080/1023666X.2017.1298012. April.
[31] E.Z. Dahmash, A. Al-Khattawi, A. Iyire, H. Al-Yami, T.J. Dennison, A. R. Mohammed, Quality by Design (QbD) based process optimisation to develop functionalised particles with modified release properties using novel dry particle coating technique, PLoS One 13 (11) (2018), e0206651.
[32] L. Nižić Nodilo, et al., A dry powder platform for nose-to-brain delivery of dexamethasone: formulation development and nasal deposition studies, Pharmaceutics 13 (6) (2021), https://doi.org/10.3390/pharmaceutics13060795.
[33] T. Waghule, N. Dabholkar, S. Gorantla, V.K. Rapalli, R.N. Saha, G. Singhvi, Quality by design (QbD) in the formulation and optimization of liquid crystalline nanoparticles (LCNPs): a risk based industrial approach, Biomed. Pharmacother. 141 (2021), 111940, https://doi.org/10.1016/j.biopha.2021.111940.
[34] S. Beg, M.S. Hasnain, M. Rahman, S. Swain, Introduction to Quality by Design (QbD): Fundamentals, Principles, and Applications, Elsevier Inc., 2019.
[35] X. Xu, M.A. Khan, D.J. Burgess, A quality by design (QbD) case study on liposomes containing hydrophilic API: I. Formulation, processing design and risk assessment, Int. J. Pharm. 419 (1–2) (2011) 52–59, https://doi.org/10.1016/j.ijpharm.2011.07.012.
[36] V. Mishra, S. Thakur, A. Patil, A. Shukla, Quality by design (QbD) approaches in current pharmaceutical set-up, Expet Opin. Drug Deliv. 15 (8) (2018) 737–758, https://doi.org/10.1080/17425247.2018.1504768.
[37] S.F.A. Tarawneh, et al., Mechanistic modelling of targeted pulmonary delivery of dactinomycin iron oxide loaded nanoparticles for lung cancer therapy, Pharmaceut. Dev. Technol. (2022) 1–35, no. just-accepted.
[38] National Library of medicine, Carbamazepine, 2021. https://pubchem.ncbi.nlm.nih.gov/compound/Carbamazepine#section=Boiling-Point. (Accessed 1 December 2021).
[39] M.M.J. Lowes, M.R. Caira, A.P. Lötter, J.G. Van Der Watt, Physicochemical properties and X-ray structural studies of the trigonal polymorph of carbamazepine, J. Pharmaceut. Sci. 76 (9) (1987) 744–752.
[40] G.E. Yassin, R.I. Amer, A.M. Fayez, Carbamazepine loaded vesicular structures for enhanced brain targeting via intranasal route: optimization, in vitro evaluation, and in vivo study, Int. J. Appl. Pharm. 11 (4) (2019) 264–274, https://doi.org/10.22159/ijap.2019v11i4.33474.
[41] P.R.M. Bittencourt, C.M. Gracia, R. Martins, A.G. Fernandas, H.W. Diekmann, W. Jung, Phenytoin and carbamazepine decrease oral bioavailability of praziquantel, Neurology 42 (3) (1992) 492.
[42] S. Liu, S. Yang, P.C. Ho, Intranasal administration of carbamazepine-loaded carboxymethyl chitosan nanoparticles for drug delivery to the brain, Asian J. Pharm. Sci. 13 (1) (2018) 72–81, https://doi.org/10.1016/j.ajps.2017.09.001.
[43] E. Gavini, et al., Nasal administration of Carbamazepine using chitosan microspheres: in vitro/in vivo studies, Int. J. Pharm. 307 (1) (2006) 9–15, https://doi.org/10.1016/j.ijpharm.2005.09.013.
[44] G.A. Morris, J. Castile, A. Smith, G.G. Adams, S.E. Harding, Macromolecular conformation of chitosan in dilute solution: a new global hydrodynamic approach, Carbohydr. Polym. 76 (4) (2009) 616–621.
[45] ICH, Validation of analytical procedures: text and methodology Q2(R1), Int. Conf. Harmon. Tech. Requir. Regist. Pharm. Hum. Use 4 (2005).
[46] J. Deng, S. Staufenbiel, R. Bodmeier, Evaluation of a biphasic in vitro dissolution test for estimating the bioavailability of carbamazepine polymorphic forms, Eur. J. Pharmaceut. Sci. 105 (2017) 64–70, https://doi.org/10.1016/j.ejps.2017.05.013.
[47] J. Kaur, et al., A hand-held apparatus for 'nose-only' exposure of mice to inhalable microparticles as a dry powder inhalation targeting lung and airway macrophages, Eur. J. Pharmaceut. Sci. 34 (1) (2008) 56–65, https://doi.org/10.1016/j.ejps.2008.02.008.
[48] R.J. Racine, Modification of seizure activity by electrical stimulation: II. Motor seizure, Electroencephalogr. Clin. Neurophysiol. 32 (3) (1972) 281–294.
[49] Q. Jarrar, R. Ayoub, S. Moshawih, Y. Jarrar, J. Jilani, Synthesis and biological evaluation of hydroxypropyl ester of mefenamic acid as a promising prodrug, Lett. Drug Des. Discov. 20 (2) (2023) 1–9, https://doi.org/10.2174/1570180819666220330160134.
[50] R. Ayoub, et al., Synthesis of novel esters of mefenamic acid with pronounced anti-nociceptive effects and a proposed activity on GABA, opioid and glutamate receptors, Eur. J. Pharmaceut. Sci. (2021), 105865.
[51] F. Alregeb, F. Khalili, B. Sweileh, D.K. Ali, Synthesis and characterization of chelating hyperbranched polyester nanoparticles for Cd (II) ion removal from water, Molecules 27 (12) (2022) 3656, https://doi.org/10.3390/molecules27123656.
[52] H.S. Alyami, et al., Taste masking of promethazine hydrochloride using l-arginine polyamide-based nanocapsules, Molecules 28 (no. 2) (2023), https://doi.org/10.3390/molecules28020748.
[53] E.Z. Dahmash, D.K. Ali, H.S. Alyami, H. Abdulkarim, M.H. Alyami, A.H. Aodah, Novel thymoquinone nanoparticles using poly(ester amide) based on L-arginine-targeting pulmonary drug delivery, Polymers 14 (6) (2022), https://doi.org/10.3390/polym14061082.
[54] M.H. Alyami, E.Z. Dahmash, D.K. Ali, H.S. Alyami, H. AbdulKarim, S.A. Alsudir, Novel fluticasone propionate and salmeterol fixed-dose combination nano-encapsulated particles using polyamide based on L-lysine, Pharmaceuticals 15 (3) (2022) 321.
[55] H. AbdulKarim, D.K. Ali, E. Taybeh, H.S. Alyami, S.M. Assaf, E.Z. Dahmash, Novel poly (ester amide) derived from tyrosine amino acid for targeted pulmonary drug delivery of fluticasone propionate, J. Appl. Polym. Sci. (2023), e53672.
[56] Y. Javadzadeh, B. Jafari-Navimipour, A. Nokhodchi, Liquisolid technique for dissolution rate enhancement of a high dose water-insoluble drug (carbamazepine), Int. J. Pharm. 341 (1–2) (2007) 26–34.
[57] R. Surekha, T. Sumathi, An efficient encapsulation of thymoquinone using solid lipid nanoparticle for brain targeted drug delivery: physicochemical characterization, pharmacokinetics and bio-distribution studies, Int. J. Pharm. Clin. Res. 8 (12) (2016) 1616–1624.
[58] S. Maraghechi, J.P.M. Hoefnagels, R.H.J. Peerlings, M.G.D. Geers, Correction of scan line shift artifacts in scanning electron microscopy: an extended digital image correlation framework, Ultramicroscopy 187 (2018) 144–163, https://doi.org/10.1016/j.ultramic.2018.01.002.
[59] J. Zhao, X. Liu, M. B. T.-E. of S. in the E. (Second E. Oliver, in: M.J. Goss (Ed.), Electron Microscopic Methods (TEM, SEM and Energy Dispersal Spectroscopy), Academic Press, Oxford, 2023, pp. 575–588.
[60] H.K. Mukhopadhyay, et al., Preparation and characterization of polymethacrylate-based matrix microspheres of carbamazepine using solvent evaporation method, FARMACIA 62 (1) (2014) 137–158.